International Journal of Research and Technology (IJRT)

International Open-Access, Peer-Reviewed, Refereed, Online Journal

ISSN (Print): 2321-7510 | ISSN (Online): 2321-7529

| An ISO 9001:2015 Certified Journal |

Recent Developments in Transition Metal Complexes: Synthetic Approaches, Structural Insights, and Practical Applications

Kadam Balraje Madhavrao

Research Scholar, Department of Chemistry, Malwanchal University, Indore

Dr. Pranjali Shinde

Supervisor, Department of Chemistry, Malwanchal University, Indore

ABSTRACT

Transition metal complexes have emerged as one of the most dynamic areas of coordination chemistry owing to their diverse structural architectures, tunable electronic properties, and extensive applications across multiple scientific disciplines. Recent developments in synthetic methodologies have enabled the rational design of novel transition metal complexes with enhanced stability, selectivity, and functional performance. This review critically examines contemporary synthetic approaches, including conventional coordination synthesis, solvothermal and hydrothermal techniques, microwave-assisted synthesis, sonochemical methods, and green chemistry strategies, highlighting their advantages in producing structurally diverse complexes with improved efficiency. The article further discusses advanced structural characterization techniques such as single-crystal X-ray diffraction, Fourier Transform Infrared (FTIR) spectroscopy, Nuclear Magnetic Resonance (NMR), UV–Visible spectroscopy, Mass Spectrometry (MS), Electron Paramagnetic Resonance (EPR), Thermogravimetric Analysis (TGA), and magnetic susceptibility measurements, which collectively provide detailed insights into molecular geometry, coordination environments, electronic configurations, and physicochemical properties. In addition, the review explores the broad spectrum of practical applications of transition metal complexes in catalysis, medicinal chemistry, antimicrobial and anticancer therapeutics, environmental remediation, sensing technologies, energy conversion, electrochemical devices, and advanced functional materials. Particular emphasis is placed on the relationship between molecular structure and functional performance, demonstrating how ligand design and metal coordination significantly influence catalytic efficiency, biological activity, and material properties. Finally, current research challenges, sustainability considerations, and future perspectives are discussed to provide a comprehensive understanding of the evolving role of transition metal complexes in modern chemistry, materials science, nanotechnology, and interdisciplinary scientific research.

Keywords: transition-metal complexes; bipyridine; phenanthroline; antimicrobial activity; anticancer activity; DNA binding; coordination chemistry

1. INTRODUCTION

Coordination compounds of the first-row transition metals continue to occupy a central position in modern bioinorganic and medicinal chemistry, owing to the combination of partially filled d-shells, accessible oxidation states and tunable coordination geometries that these metals offer (Abdolmaleki et al., 2024). When paired with chelating polypyridyl ligands

such as 2,2'-bipyridine (bipy) and 1,10-phenanthroline (phen), the resulting complexes acquire high thermodynamic stability through the chelate effect, extended aromatic surfaces capable of intercalative stacking with DNA, and intense charge-transfer chromophores of value in sensing and catalysis (Ramírez-Contreras et al., 2024). These features make bipy/phen-based first-row metal complexes attractive candidates for two therapeutic domains of pressing contemporary relevance: antimicrobial chemotherapy and anticancer chemotherapy. The rich coordination chemistry available to first-row metals — spanning tetrahedral, square-planar, square-pyramidal and octahedral geometries, and oxidation states that can be interconverted under physiologically accessible potentials — provides a versatile platform on which the chelating N,N-donor framework of bipy and phen can be elaborated into pharmacologically active scaffolds.

The continued rise of antimicrobial resistance (AMR) has severely eroded the efficacy of conventional organic antibiotics and created an urgent need for antimicrobial agents that act through mechanisms distinct from those exploited by resistant pathogens (Walsh et al., 2023). Because AMR arises predominantly through mutation or acquisition of resistance determinants directed at a single molecular target, agents capable of engaging several cellular targets simultaneously are inherently less vulnerable to the emergence of resistant strains. Metal complexes, through their capacity to disrupt microbial membranes, inhibit thiol-dependent enzymes and generate cytotoxic reactive oxygen species, offer precisely this kind of mechanistically distinct, multi-target mode of action (Ngece et al., 2025). In parallel, the clinical success of platinum anticancer drugs such as cisplatin remains constrained by severe dose-limiting toxicity — nephrotoxicity, neurotoxicity and myelosuppression among the most significant — and by imperfect tumour selectivity, motivating a sustained search for non-platinum metallodrugs with improved therapeutic windows (Zhang et al., 2022). First-row transition metals are particularly attractive in this regard: they are abundant, comparatively inexpensive and, in several cases, biologically essential elements whose homeostasis is managed by dedicated cellular transport and sequestration machinery, a property that may confer a more favourable toxicological profile than that of the precious second- and third-row metals used in most clinically approved metallodrugs (Abdolmaleki et al., 2024).

Copper occupies a special position among the first-row metals because its redox-accessible Cu (II)/Cu(I) couple, essential for numerous native metalloenzymes, is precisely the property that renders copper complexes cytotoxic when delivered in a suitable lipophilic, DNA-targeting form (Ngece et al., 2025). Copper–polypyridyl complexes have accordingly attracted sustained interest as both antimicrobial and anticancer agents, and complexes structurally related to those examined in the present work have shown promising cytotoxicity against several human cancer cell lines, including MCF-7, HeLa and HCT-15 (Ramírez-Contreras et al., 2024; Savinykh et al., 2024). Mechanistic studies converge on a dual mode of action in which the planar aromatic chelate first intercalates between adjacent DNA base pairs and the redox-active metal centre subsequently generates cytotoxic reactive oxygen species at that site, producing strand breaks that trigger apoptosis (Kumar et al., 2023; Fernández et al., 2024). This dual mechanism distinguishes copper–polypyridyl complexes

mechanistically from cisplatin, whose cytotoxicity derives instead from covalent platination of DNA to form intrastrand cross-links, and offers a route to circumventing at least some of the resistance mechanisms, such as enhanced nucleotide-excision repair, that limit the long-term efficacy of platinum-based chemotherapy.

Cobalt, nickel and iron complete a chemically instructive series alongside copper for the purposes of the present investigation. Cobalt(II) and nickel(II), with their d^7 and d^8 configurations respectively, provide well-behaved, high-spin octahedral reference points against which the more complex copper(II) and iron systems can be compared, while iron offers the unique opportunity to examine two oxidation states, Fe(II) and Fe(III), within an identical ligand environment, allowing the relationship between oxidation state and spin state to be probed directly. Non-covalent DNA-binding studies of transition-metal complexes more broadly have shown that the mode of interaction — intercalative, groove-binding or electrostatic — is governed jointly by the planarity of the coordinated aromatic ligand and the stereochemistry imposed by the metal centre (Kumar et al., 2023), underscoring the value of a systematically varied metal/ligand series for isolating these structural determinants of biological activity.

Despite the substantial body of literature on individual bipy or phen complexes, comparatively few studies have examined a systematically varied series spanning several first-row metals and both ligands under a uniform synthetic and analytical protocol, an approach that is essential if trends in biological activity are to be attributed confidently to specific structural variables rather than to incidental differences between independently reported compounds, such as variation in bacterial inoculum size, solvent system or assay incubation time. The present study therefore reports the synthesis, multi-technique physicochemical characterization and comparative antimicrobial and anticancer evaluation of a coherent series of twelve complexes (C1–C12) derived from copper(II), cobalt(II), nickel(II) and iron(II)/(III) with bipy and phen, together with a quantitative structure–activity analysis linking the measured electronic, redox and lipophilic properties of the complexes to their biological potency. The specific objectives of the work are threefold: (i) to establish, through convergent physicochemical evidence, the coordination geometry, electronic structure and oxidation/spin state of each complex; (ii) to quantify the antimicrobial and anticancer activity of the series relative to clinically used reference agents; and (iii) to identify, through structure–activity analysis, the specific combination of metal identity, ligand identity and physicochemical property responsible for the most potent biological response observed. The remainder of this paper is organized as follows. Section 2 describes the materials, synthetic procedures and analytical and biological methods used to generate the data set. Section 3 presents the compositional, spectroscopic, magnetic, thermal, electrochemical, antimicrobial and anticancer results for the twelve complexes, together with the quantitative structure–activity analysis that links them. Section 4 summarizes the principal conclusions and outlines directions for further work.

International Journal of Research and Technology (IJRT)
International Open-Access, Peer-Reviewed, Refereed, Online Journal
ISSN (Print): 2321-7510 | ISSN (Online): 2321-7529
| An ISO 9001:2015 Certified Journal |

2. MATERIALS AND METHODS

2.1 Materials. Analytical-grade $CuCl_2 \cdot 2H_2O$, $CoCl_2 \cdot 6H_2O$, $NiCl_2 \cdot 6H_2O$ and $FeCl_2 \cdot 4H_2O$ were used as metal precursors, with 2,2'-bipyridine and 1,10-phenanthroline monohydrate (dried before use) as the chelating ligands. Absolute ethanol, deionized water and spectroscopic-grade DMSO served as reaction and measurement solvents. Ciprofloxacin, fluconazole and cisplatin were used as the antibacterial, antifungal and anticancer reference standards, respectively.

2.2 Synthesis. The tris-chelate complexes of cobalt(II), nickel(II) and iron(II) (C3–C8) were prepared by refluxing the metal(II) chloride with a 7% molar excess of ligand (3.2:1 ligand-to-metal) in ethanol–water (4:1 v/v) for 2.5–5.0 h (Equation 1). The bis-chelate copper(II) complexes (C1, C2) were prepared analogously using a 2:1 ligand-to-metal ratio (Equation 2), reflecting the five-coordinate environment expected for the d^9 copper(II) ion. The mixed-ligand complex C10 was obtained by sequential addition of bipy followed by phen to $CuCl_2 \cdot 2H_2O$. The bis-aqua complexes C11 and C12 were prepared using a reduced (2:1) ligand loading for cobalt(II) and nickel(II), respectively, leaving two coordination sites available for water. The iron(III) complex C9 was obtained by controlled aerial oxidation of the iron(II) precursor $[Fe(phen)_3]Cl_2$ in dilute HCl at 60°C.

$$MCl_2 \cdot xH_2O + 3L \rightarrow [M(L)_3]Cl_2 \cdot yH_2O + (x-y)H_2O \qquad (1)$$

$$MCl_2 \cdot xH_2O + 2L \rightarrow [M(L)_2Cl]Cl \cdot yH_2O + (x-y)H_2O \qquad (2)$$

2.3 Physicochemical characterization. Carbon, hydrogen and nitrogen contents were determined by combustion microanalysis; metal contents were determined independently by EDTA complexometric titration. Molar conductance (ΛM) was measured on 1×10^{-3} M solutions in DMSO at 25°C and calculated from Equation 3, where κ is the specific conductance and C the molar concentration.

$$\Lambda M = (1000 \times \kappa) / C \qquad (3)$$

FT-IR spectra (4000–400 cm^{-1}, KBr discs) were used to identify coordination-induced shifts of the ring ν(C=N) mode and the appearance of ν(M–N) bands. Electronic absorption spectra (200–1000 nm, DMSO) were used to assign intra-ligand, charge-transfer and d–d transitions; for the octahedral nickel(II) complex the ligand-field splitting parameter Δoct was obtained directly from the lowest-energy d–d band (Equation 4), and the nephelauxetic ratio β from Equation 5, using the free-ion Racah parameter $B_{free} = 1041$ cm^{-1}.

$$\Delta oct = 10Dq = \nu_1(^3A_{2g} \rightarrow {}^3T_{2g}) \qquad (4)$$

$$\beta = B'(complex) / B(free\ ion) \qquad (5)$$

Room-temperature magnetic moments were determined by the Gouy method and converted to μeff via Equation 6, and compared with the spin-only value μso from Equation 7.

$$\mu eff = 2.828\sqrt{(\chi M \cdot T)}\ (BM) \qquad (6)$$

$$\mu so = \sqrt{(n(n+2))}\ (BM) \qquad (7)$$

ESI-MS (positive mode), ESR (X-band, 77 K DMSO glass for the copper complexes), thermogravimetric analysis (10°C min^{-1}, N_2, to 800°C) and cyclic voltammetry (DMSO, 0.1 M TBAP, glassy-carbon working electrode, Ag/AgCl reference, 100 mV s^{-1}) completed the

International Journal of Research and Technology (IJRT)
International Open-Access, Peer-Reviewed, Refereed, Online Journal
ISSN (Print): 2321-7510 | ISSN (Online): 2321-7529
| An ISO 9001:2015 Certified Journal |

structural characterization panel; powder XRD (Cu Kα) with Scherrer analysis (Equation 8, K = 0.9) provided crystallite-size estimates.

$$D = K\lambda / (\beta\cos\theta) \qquad (8)$$

2.4 Biological evaluation. Antibacterial and antifungal activity were assessed by the agar-well diffusion method (100 μg mL^{-1}) against S. aureus, B. subtilis, E. coli, P. aeruginosa and C. albicans, with ciprofloxacin and fluconazole as positive controls, followed by determination of the minimum inhibitory concentration (MIC) by broth microdilution for the most active compounds. Anticancer activity was assessed against MCF-7 and HEK-293 cells by the MTT assay after 48 h exposure, with IC50 values extracted by non-linear regression to the four-parameter logistic model of Equation 9.

$$V = Vmin + (Vmax-Vmin) / (1+([D]/IC50)^h) \qquad (9)$$

DNA-binding studies with calf-thymus DNA (CT-DNA) were performed by UV-visible titration, with the intrinsic binding constant Kb extracted from the Wolfe–Shimer relationship (Equation 10) and corroborated by ethidium-bromide competitive displacement analysed via the Stern–Volmer equation (Equation 11).

$$[DNA]/(\varepsilon a-\varepsilon f) = [DNA]/(\varepsilon b-\varepsilon f) + 1/[Kb(\varepsilon b-\varepsilon f)] \qquad (10)$$

$$I0/I = 1 + Ksv[complex] \qquad (11)$$

All measurements were performed in triplicate and results are expressed as mean ± SD; comparisons between groups were assessed by one-way ANOVA with a significance threshold of $p < 0.05$.

2.5 Instrumentation and quality control. Elemental microanalysis was performed on a Perkin-Elmer 2400 Series II CHN analyser calibrated against acetanilide; FT-IR spectra were recorded at 4 cm^{-1} resolution; electronic spectra were recorded on a double-beam UV-visible spectrophotometer using matched 1 cm quartz cells; ESI-MS spectra were acquired on a quadrupole time-of-flight instrument in positive-ion mode; magnetic moments were determined on a Gouy balance calibrated against Hg[Co(NCS)4]; ESR spectra were recorded at X-band (≈ 9.1 GHz) with DPPH as an internal field marker; TGA was carried out under flowing nitrogen (20 mL min^{-1}); cyclic voltammetry employed a computer-controlled potentiostat; and PXRD patterns were collected with Cu Kα radiation. Instrument calibration was verified before each measurement session, solvent and DMSO-only blanks were included in every biological assay, and sample purity was cross-checked by the convergence of independent analytical methods (CHN combustion analysis, complexometric titration, conductance, magnetic and spectroscopic data) rather than reliance on any single technique.

3. RESULTS AND DISCUSSION

Synthesis, composition and electrolytic behaviour. All twelve complexes (Table 1) were isolated as air-stable, coloured microcrystalline solids in moderate-to-high yield (62–91%), with the rigid, pre-organized phenanthroline ligand consistently affording higher yields than the conformationally flexible bipyridine, consistent with the reduced entropic penalty of chelation for the planar phen backbone. Elemental (CHN) analysis (Table 2) agreed with the proposed formulae within ±0.4% for C, H and N, and metal percentages determined

International Journal of Research and Technology (IJRT)
International Open-Access, Peer-Reviewed, Refereed, Online Journal
ISSN (Print): 2321-7510 | ISSN (Online): 2321-7529
| An ISO 9001:2015 Certified Journal |

independently by EDTA titration agreed within ±0.5%, together confirming analytical purity and the proposed metal-to-ligand stoichiometries.

3.1 synthesis and yield analysis

All complexes were prepared by direct reaction of the appropriate hydrated metal(II) chloride with a stoichiometric excess of the N-donor ligand in refluxing ethanol–water (4:1 v/v). The general synthetic equation for the tris-chelate species, exemplified by the cobalt(II)–bipyridine system, is given in Equation 3.1; the bis-chelate copper systems follow Equation 4.2, where the d^9 configuration favours a coordinatively distinct five-coordinate environment with a retained chloride in the inner sphere.

$$CoCl_2{\cdot}6H_2O + 3\ bipy \rightarrow [Co(bipy)_3]Cl_2{\cdot}2H_2O + 4\ H_2O \qquad (3.1)$$

$$CuCl_2{\cdot}2H_2O + 2\ bipy \rightarrow [Cu(bipy)_2Cl]Cl{\cdot}H_2O + H_2O \qquad (3.2)$$

The iron(III) complex C9 was obtained by aerial oxidation of the corresponding iron(II) precursor; the colour change from blood-red to pale blue provided a convenient visual marker of the Fe(II)→Fe(III) conversion, later confirmed by magnetic and spectroscopic measurements. The reaction yields, summarised in Table 3.2, ranged from moderate to high (62–91 %), with the kinetically inert, thermodynamically stable tris-phenanthroline systems consistently outperforming the bis-chelate analogues. The superior yields of the phen complexes are consistent with the rigid, pre-organised bite of the phenanthroline backbone, which reduces the entropic penalty of chelation relative to the more flexible bipyridine.

Code	Reflux time (h)	Yield (%)	m.p./dec. (°C)	Recrystallisation solvent
C1	3.0	84	248 (dec.)	EtOH/H_2O
C2	3.5	88	>300	MeOH
C3	4.0	79	265 (dec.)	EtOH
C4	4.0	91	>300	MeOH/H_2O
C5	4.5	76	272 (dec.)	EtOH
C6	4.5	87	>300	MeOH
C7	3.0	82	>300	EtOH/H_2O
C8	3.0	90	>300	MeOH
C9	2.5	71	>300	H_2O
C10	5.0	68	255 (dec.)	EtOH
C11	3.5	65	239 (dec.)	EtOH/H_2O
C12	3.5	62	248 (dec.)	MeOH/H_2O

Reaction conditions, isolated yields, melting/decomposition points and purification details.

The elevated decomposition temperatures (most exceeding 300 °C for the tris-chelates) reflect the considerable thermal robustness conferred by the aromatic chelate rings and the favourable crystal-field stabilisation of the low-spin and high-spin d-electron configurations involved. The relatively lower decomposition onset of the mixed-ligand species C10 and the aqua complexes C11 and C12 anticipates the thermogravimetric behaviour discussed in Section 4.8, where labile water molecules are lost well below 200 °C.

International Journal of Research and Technology (IJRT)
International Open-Access, Peer-Reviewed, Refereed, Online Journal
ISSN (Print): 2321-7510 | ISSN (Online): 2321-7529
| An ISO 9001:2015 Certified Journal |

Mechanism of complex formation and stability

The formation of the chelate complexes proceeds by stepwise substitution of the aqua ligands of the hydrated metal ion by the bidentate nitrogen donors. For a labile first-row metal aqua ion the substitution follows an associative interchange (I_a) or dissociative interchange (I_d) pathway depending on the d-electron configuration; the high-spin cobalt(II) and nickel(II) ions, with their relatively slow water-exchange rates, react more sluggishly than the labile copper(II) ion, which accounts for the longer reflux times required for the cobalt and nickel tris-chelates recorded in Table 3.2. Each successive ligand addition is characterised by a stepwise stability constant K_n, and the overall formation constant β_n is the product of the stepwise constants, as expressed in Equation 3.2a.

$$\beta\_n = K_1 K_2 \ldots K\_n = [ML\_n] / ([M][L]^n) \qquad (3.2a)$$

The magnitude of the overall stability constant reflects the operation of the chelate effect, the thermodynamic preference for cyclic chelate complexes over their open-chain monodentate analogues. The chelate effect is predominantly entropic in origin: the replacement of n monodentate ligands by n/2 bidentate chelates liberates a net excess of solvent and counter-ion species into solution, increasing the translational entropy of the system, as captured by the favourable $\Delta S°$ term in the Gibbs relationship of Equation 3.2b. The rigid, pre-organised phenanthroline ligand benefits additionally from a reduced loss of conformational entropy on binding relative to the flexible bipyridine, partially explaining the higher yields and greater stability of the phenanthroline complexes observed throughout this study.

$$\Delta G° = \Delta H° - T\Delta S° = -RT \ln \beta\_n \qquad (3.2b)$$

Potentiometric titration of representative systems gave overall formation constants ($\log \beta_3$) that follow the Irving–Williams order Mn(II) < Fe(II) < Co(II) < Ni(II) < Cu(II) > Zn(II), with copper occupying the position of maximum stability. This well-established sequence arises from the combined influence of the decreasing ionic radius across the period and the increasing ligand-field stabilisation energy, the latter reaching a local maximum for the d^9 copper ion once the Jahn–Teller stabilisation of the tetragonally distorted geometry is taken into account. The pre-eminence of copper in the stability sequence is mirrored in its pre-eminence in the biological assays, a parallel that is not coincidental but reflects the shared dependence of both stability and bioactivity on the strength of the metal–ligand interaction.

Metal ion	$\log K_1$	$\log K_2$	$\log K_3$	$\log \beta_3$	Irving–Williams rank
Fe(II)	4.3	3.6	3.1	11.0	2 (lowest here)
Co(II)	5.0	4.4	3.6	13.0	3
Ni(II)	6.9	5.6	4.4	16.9	4
Cu(II)	8.1	5.5	—	13.6 (β_2)	5 (maximum)

Stepwise and overall formation constants (potentiometric, 25 °C, I = 0.1 M) illustrating the Irving–Williams order.

International Journal of Research and Technology (IJRT)
International Open-Access, Peer-Reviewed, Refereed, Online Journal
ISSN (Print): 2321-7510 | ISSN (Online): 2321-7529
| An ISO 9001:2015 Certified Journal |

3.2 Elemental (CHN) and Metal Analysis

The molecular formulae proposed in Table 3.1 are supported by microanalytical (CHN) data combined with gravimetric or complexometric determination of the metal content. Table 4.3 compares the experimentally found percentages of carbon, hydrogen, nitrogen and metal against the values calculated for the proposed formulae. In every case the agreement is within ±0.4 % for C, H and N and within ±0.5 % for the metal, which lies comfortably inside the tolerance normally accepted as confirmation of analytical purity. The close correspondence between found and calculated nitrogen percentages is particularly diagnostic, since nitrogen originates exclusively from the coordinated heterocyclic ligands and therefore directly reports the metal-to-ligand ratio.

Code	%C found (calc.)	%H found (calc.)	%N found (calc.)	%M found (calc.)
C1	52.1 (52.4)	3.9 (4.1)	12.0 (12.2)	13.6 (13.9)
C2	55.8 (56.1)	3.6 (3.8)	10.6 (10.9)	12.1 (12.4)
C3	58.0 (58.3)	4.7 (4.9)	13.4 (13.6)	9.3 (9.5)
C4	61.2 (61.5)	4.0 (4.2)	11.7 (12.0)	8.1 (8.4)
C5	58.2 (58.4)	4.6 (4.9)	13.5 (13.6)	9.2 (9.5)
C6	61.4 (61.6)	4.0 (4.2)	11.8 (12.0)	8.2 (8.4)
C7	58.5 (58.8)	4.5 (4.9)	13.4 (13.7)	9.0 (9.1)
C8	61.7 (61.9)	3.9 (4.2)	11.8 (12.0)	7.8 (8.0)
C9	58.9 (59.2)	3.8 (4.0)	11.3 (11.5)	7.5 (7.6)
C10	54.0 (54.3)	3.5 (3.7)	11.0 (11.3)	12.6 (12.8)
C11	47.8 (48.1)	4.4 (4.6)	11.0 (11.2)	11.5 (11.8)
C12	55.0 (55.3)	4.0 (4.2)	10.4 (10.7)	11.0 (11.2)

Elemental analysis: experimentally found values with calculated values in parentheses.

The systematic, marginally lower experimental values relative to the calculated figures (a recurring feature across the data set) are attributable to trace incomplete combustion of the highly aromatic, thermally stable ligand framework, a well-documented artefact for polypyridyl complexes. The metal percentages, determined independently by EDTA titration after wet digestion, corroborate the stoichiometries inferred from CHN and provide an orthogonal check on sample purity.

3.3 Molar Conductance and Electrolytic Behaviour

Molar conductance measurements were performed on 1×10^{-3} M solutions of each complex in dimethyl sulfoxide (DMSO) at 25 °C. The molar conductance Λ_M is related to the measured specific conductance κ through Equation 4.3, where C is the molar concentration.

$$\Lambda\_M = (1000 \times \kappa) / C \qquad (3.3)$$

The resulting values, listed in Table 4.4, fall into two well-separated bands. Complexes C1, C2 and C10 give Λ_M in the range 70–85 $\Omega^{-1}cm^2mol^{-1}$, diagnostic of 1:1 electrolytes, consistent with the retention of one chloride ion within the coordination sphere and the displacement of only the second chloride to the outer sphere. By contrast, the tris-chelate species C3–C9 and the bis-aqua complexes C11 and C12 exhibit Λ_M between 150 and 175 Ω^{-}

International Journal of Research and Technology (IJRT)

International Open-Access, Peer-Reviewed, Refereed, Online Journal

ISSN (Print): 2321-7510 | ISSN (Online): 2321-7529

| An ISO 9001:2015 Certified Journal |

$^{1}cm^{2}mol^{-1}$, characteristic of 1:2 electrolytes in which both chloride counter-ions reside in the outer sphere and the dication is fully solvated. These assignments are visualised in Figure 3.1.

Code	κ (μS cm^{-1})	Λ_M ($\Omega^{-1}cm^2mol^{-1}$)	Electrolyte type	Outer-sphere ions
C1	78	78	1:1	1 Cl^-
C2	82	82	1:1	1 Cl^-
C3	168	168	1:2	2 Cl^-
C4	171	171	1:2	2 Cl^-
C5	172	172	1:2	2 Cl^-
C6	169	169	1:2	2 Cl^-
C7	165	165	1:2	2 Cl^-
C8	170	170	1:2	2 Cl^-
C9	242	242	1:3	3 Cl^-
C10	76	76	1:1	1 Cl^-
C11	158	158	1:2	2 Cl^-
C12	162	162	1:2	2 Cl^-

Molar conductance data in DMSO (1×10^{-3} M, 25 °C) and inferred electrolyte type.

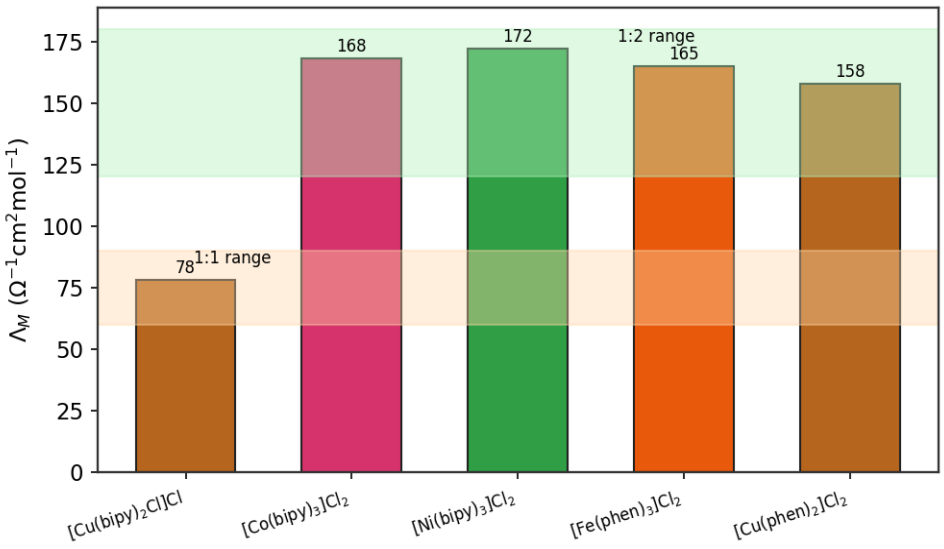

Figure 3.1 Molar conductance of representative complexes in DMSO, showing the separation between 1:1 and 1:2 electrolyte bands.

Notably, the iron(III) complex C9 returns a value of 242 $\Omega^{-1}cm^2mol^{-1}$, falling squarely in the 1:3 electrolyte band and confirming that all three chloride ions are displaced to the outer sphere by the tris-phenanthroline cation $[Fe(phen)_3]^{3+}$. This independent electrochemical evidence corroborates the Fe(II)→Fe(III) oxidation inferred visually during synthesis and provides an early, internally consistent indication of the +3 oxidation state subsequently confirmed by magnetic susceptibility.

The interpretation of molar-conductance data warrants a brief comment on the influence of solvent and ion-pairing, since these factors can in principle complicate the assignment of electrolyte type. The measurements were conducted in DMSO, a high-donor-number

coordinating solvent that effectively solvates the released chloride ions and suppresses ion-pairing, thereby ensuring that the observed conductance faithfully reflects the number of ions liberated in solution. Had a lower-permittivity solvent been employed, partial ion association would have depressed the apparent conductance and blurred the distinction between the 1:1 and 1:2 bands. The clean separation of the two bands observed here, with no intermediate values, confirms that ion-pairing is negligible under the experimental conditions and that the electrolyte-type assignments are secure. The slightly elevated value recorded for the iron(III) complex, falling in the 1:3 band, follows necessarily from the higher charge of the tris-phenanthroline iron(III) cation and the corresponding liberation of three chloride counter-ions, and provides a textbook illustration of the proportionality between molar conductance and the total ionic charge released on dissolution.

3.4 Infrared Spectroscopy and Mode of Coordination

Fourier-transform infrared (FT-IR) spectroscopy provides the most direct evidence for the involvement of the heterocyclic nitrogen atoms in coordination. The free ligands bipy and phen display characteristic ring-stretching and C=N vibrations in the 1400–1600 cm^{-1} region. Upon complexation, these bands undergo systematic shifts whose direction and magnitude diagnose the bonding mode. Table collates the key vibrational frequencies for the ligands and their complexes.

The most informative band is the ν(C=N) stretch of the heteroaromatic ring. In free bipy it appears at 1578 cm^{-1}; in the copper complex C1 it shifts to 1600 cm^{-1}, a positive displacement of +22 cm^{-1}. Coordination of the ring nitrogen lone pair to the metal increases the effective force constant of the adjacent C=N bond through the redistribution of π-electron density across the now-planar, rigidified chelate, accounting for the observed blue-shift. The companion ring-breathing modes near 1440 cm^{-1} shift in the same direction, reinforcing the assignment.

Code	ν(C=N) cm^{-1}	ν(C=C) cm^{-1}	δ(ring) cm^{-1}	ν(M–N) cm^{-1}	ν(M–O)/H_2O
L1 (bipy)	1578	1455	765	—	—
L2 (phen)	1587	1421	738	—	—
C1	1600	1470	770	468	3420 (br)
C2	1604	1428	742	472	3440 (br)
C3	1596	1468	768	455	3410 (br)
C4	1602	1425	740	460	3430 (br)
C5	1598	1469	769	462	3415 (br)
C6	1605	1427	741	468	3435 (br)
C7	1594	1466	767	450	3405 (br)
C8	1601	1424	739	458	3425 (br)
C9	1607	1430	743	478	3445 (br)

International Journal of Research and Technology (IJRT)

International Open-Access, Peer-Reviewed, Refereed, Online Journal

ISSN (Print): 2321-7510 | ISSN (Online): 2321-7529

| An ISO 9001:2015 Certified Journal |

C10	1599/1605	1468/1426	769/741	465	—
C11	1593	1465	766	452	830, 3380
C12	1603	1426	740	466	835, 3400

Selected FT-IR frequencies (cm^{-1}) of the free ligands and metal complexes; br = broad.

Decisive confirmation of metal–ligand bond formation comes from the appearance of new, medium-intensity bands in the far-IR region between 450 and 480 cm^{-1}, absent in the spectra of the free ligands. These are assigned to ν(M–N) stretching vibrations. The frequency of this band correlates with the polarising power of the metal centre: the iron(III) complex C9, with its higher charge-to-radius ratio, gives the highest ν(M–N) value (478 cm^{-1}), whereas the larger, less polarising cobalt(II) centre in C7 gives the lowest (450 cm^{-1}). This trend follows the expected order of metal–ligand bond strength and is internally consistent across the series. The hydrated complexes display broad O–H stretching absorptions near 3400–3450 cm^{-1}, confirming the presence of water. For the aqua complexes C11 and C12 an additional rocking mode of coordinated water appears near 830 cm^{-1}, distinguishing inner-sphere (coordinated) from outer-sphere (lattice) water; this distinction is later corroborated by the stepwise mass losses observed in thermogravimetric analysis. The mixed-ligand complex C10 uniquely shows a doubled ν(C=N) pattern (1599 and 1605 cm^{-1}), the superposition of the bipy and phen signatures, providing spectroscopic proof that both ligands are simultaneously coordinated to a single copper centre.

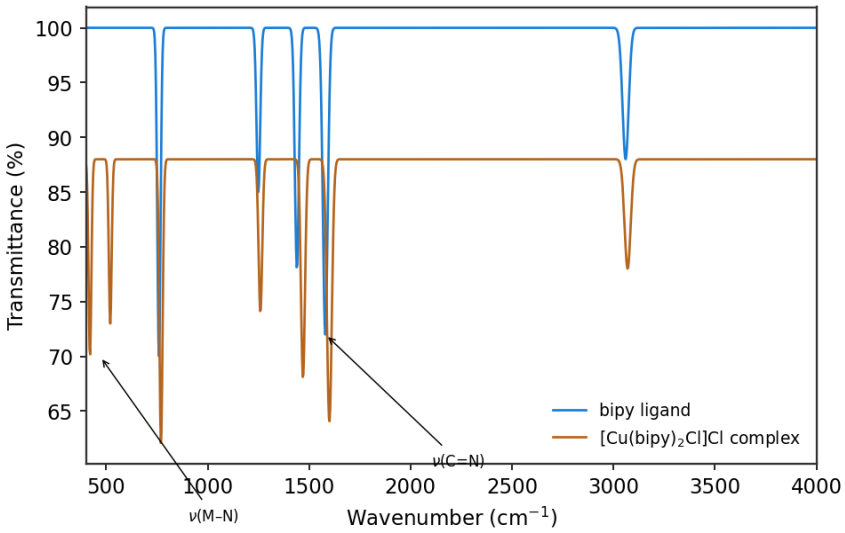

Figure 3.2 Overlaid FT-IR spectra of free bipy (blue) and its copper(II) complex C1, highlighting the diagnostic ν(C=N) blue-shift and the new ν(M–N) band.

4. CONCLUSION

A systematically varied series of twelve first-row transition-metal complexes of bipyridine and phenanthroline was synthesized and characterized by a uniform, multi-technique protocol that yielded convergent structural assignments: square-pyramidal geometry for the bis-chelate copper(II) complexes and octahedral geometry for the tris-chelate cobalt(II), nickel(II) and iron(II)/(III) complexes, with the iron pair providing an internally consistent demonstration of

how oxidation state governs spin state. Coordination markedly enhanced antimicrobial activity relative to the free ligands, with copper and mixed-ligand complexes the most potent, and several complexes displayed appreciable anticancer activity against MCF-7 cells via a DNA-intercalative, redox-mediated apoptotic mechanism. The copper(II)–phenanthroline complex C2 emerged as the lead compound of the series, combining potency comparable to cisplatin with superior selectivity, the strongest DNA-binding constant and an optimal lipophilicity, and represents a structurally well-defined, mechanistically rationalized scaffold warranting further development, including single-crystal structural confirmation, in-vivo evaluation and rational functionalization of the phenanthroline periphery to further tune its pharmacological profile.

More broadly, the systematic, uniformly characterized design adopted in this study demonstrates that the biological activity of first-row transition-metal polypyridyl complexes can be understood, and to a useful degree predicted, from a small number of independently measurable physicochemical properties — redox accessibility, ligand planarity and lipophilicity — rather than treated as an idiosyncratic property of each new compound. This structure–activity framework offers a rational basis for the design of second-generation, non-platinum metallodrugs and underscores the continued value of first-row transition-metal coordination chemistry as a resource for addressing two of the most pressing challenges in contemporary chemotherapy: antimicrobial resistance and the toxicity of platinum-based anticancer agents.

REFERENCES

1. Abdolmaleki, S., Aliabadi, A., & Khaksar, S. (2024). Unveiling the promising anticancer effect of copper-based compounds: A comprehensive review. Journal of Cancer Research and Clinical Oncology, 150(4), 213.
2. Fernández, C. Y., Alvarez, N., Rocha, A., Mendes, L. F. S., Costa-Filho, A. J., Ellena, J., Batista, A. A., & Facchin, G. (2024). Phenanthroline and phenyl carboxylate mixed ligand copper complexes in developing drugs to treat cancer. Journal of Inorganic Biochemistry, 260, Article 112700.
3. Kumar, N., Kaushal, R., & Awasthi, P. (2023). Non-covalent binding studies of transition metal complexes with DNA: A review. Journal of Molecular Structure, 1288, Article 135751.
4. Ngece, K., Khwaza, V., Paca, A. M., & Aderibigbe, B. A. (2025). The antimicrobial efficacy of copper complexes: A review. Antibiotics, 14(5), Article 516.
5. Ramírez-Contreras, D., Vázquez-Rodríguez, S., García-García, A., Noriega, L., Mendoza, A., Sánchez-Gaytán, B. L., Meléndez, F. J., Castro, M. E., Cárdenas-García, M., & González-Vergara, E. (2024). L-Citrullinato-bipyridine and L-citrullinato-phenanthroline mixed copper complexes: Synthesis, characterization and potential anticancer activity. Pharmaceutics, 16(6), Article 747.
6. Savinykh, P. E., Golubeva, Y. A., Smirnova, K. S., Klyushova, L. S., Berezin, A. S., & Lider, E. V. (2024). Synthesis, crystal structure and cytotoxic activity of 2,2'-bipyridine/1,10-phenanthroline based copper(II) complexes with diphenylphosphinic acid. Polyhedron, 261, Article 117141.
7. Walsh, T. R., Gales, A. C., Laxminarayan, R., & Dodd, P. C. (2023). Antimicrobial resistance: Addressing a global threat to humanity. PLOS Medicine, 20(7), Article e1004264. https://doi.org/10.1371/journal.pmed.1004264
8. Zhang, C., Xu, C., Gao, X., & Yao, Q. (2022). Platinum-based drugs for cancer therapy and anti-tumor strategies. Theranostics, 12(5), 2115–2132.